MP2- and RPA-Based Ab Initio Molecular Dynamics and Monte Carlo Sampling

Hutter, Jürg ; Wilhelm, Jan ; Rybkin, Vladimir V ; Ben, Mauro Del ; VandeVondele, Joost

DOI: https://doi.org/10.1007/978-3-319-42913-7_58-1

MP2 and RPA based ab initio molecular dynamics and Monte Carlo sampling

Jürg Hutter, Jan Wilhelm, Vladimir V. Rybkin, Mauro Del Ben, and Joost VandeVondele

Abstract Nonlocal correlation methods based on wavefunction theory are developed for application to condensed matter systems. These methods include MP2 and direct RPA theory as well as double hybrid functionals. Analytic gradients and stress tensors for MP2 theory in the gamma point approximation have been developed. Sampling complex systems at ambient temperature, for example liquid water, becomes possible with efficient algorithms for massively parallel computers. Results show a qualitative improvement over standard local density functionals as well as hybrid functionals.

1 Introduction

Combining ensemble sampling techniques, like molecular dynamics or Monte Carlo methods, with first-principles electronic structure theory is commonly refered to as *ab initio* molecular dynamics (AIMD) (Marx and Hutter 2009). AIMD as a modern simulation technique was started by the seminal work of Roberto Car and Michele Parrinello (Car and Parrinello 1985). The Car–Parrinello (CP) method made AIMD simulations possible for a wide range of applications. In the early years, the CP method dominated the field and became a synonym for AIMD. The original CP method was proposed using Kohn–Sham density functional theory within the pseudopotential-plane wave framework. Standard simulation protocols for CP simulations were established and used by many groups. In recent years, new

Jürg Hutter · Jan Wilhelm · Vladimir V. Rybkin
Institut für Chemie, Universität Zurich, Winterthurerstrasse 190, 8057 Zurich, e-mail: hutter@chem.uzh.ch, jan.wilhelm@chem.uzh.ch, vladimir.rybkin@chem.uzh.ch

Mauro Del Ben
Computational Research Division, Lawrence Berkeley National Laboratory, e-mail: mdelben@lbl.gov

Joost VandeVondele
Scientific Software & Libraries unit, CSCS, ETH Zürich, e-mail: joost.vandevondele@cscs.ch

developments were able to overcome limitations of the CP method while keeping all of the benefits of the original method (Hutter 2012).

With the availability of more and more computer power, it became possible to also use Monte Carlo (MC) sampling techniques (McGrath et al 2005b). In MC sampling the reuse of previous wavefunction information is much more difficult than in MD sampling. However, when atom-centered basis functions are used, this problem is considerably less severe than for example in plane wave calculations. MC sampling has advantages over MD sampling in specific situations, like the simulation of the vapour-liquid coexistance curve (McGrath et al 2005a,b), in situations where high barriers make sampling difficult (Schönherr et al 2014), or if forces are not available (Del Ben et al 2013b).

In the past, using other electronic structure methods than Kohn–Sham density functional theory was explored but never gained wide popularity. The lack of efficient implementations of correlated wavefunction methods for periodic systems and, especially, insufficient computational power to perform extensive sampling made such applications very demanding. A first step in the direction of the application of wavefunction correlation methods in AIMD was the successfull incorporation of efficient exact exchange functionals in condensed matter simulations (Todorova et al 2006; Guidon et al 2008). Only in recent years it has been possible to combine extensive sampling approaches with wavefunction correlation methods (Del Ben et al 2013b, 2015b). In this article we will summarize developments of electronic structure methods that made the application of wavefunction correlation methods in AIMD possible. We will also investigate the results from pioneering applications.

2 MP2 and RPA correlation energy methods

The generalized gradient model (GGA) within Kohn–Sham DFT had tremendous success in numerous applications. Yet, the model has significant short-comings that also influence e.g. the quality of simulations for aqueous chemistry. Most notably are the absence of van der Waals interactions and a significant self-interaction error. The former leads e.g. to a underestimation of the water density (Schmidt et al 2009; Wang et al 2011), while the latter leads to an underestimated band gap, with implications for redox chemistry (Adriaanse et al 2012) and the static dielectric constant (Schönherr et al 2014). It is possible to go beyond GGA in various ways, and improvements have been made by including various descriptors of the electronic system to yield models with improved accuracy. In an attempt to classify this progress Perdew et al (2005), employed the metaphor of a "Jacob's ladder" for which each rung of the ladder introduces more descriptors of the electronic system and yields models with improved accuracy. This ladder has currently five rungs which include as descriptors (1) the electronic density, (2) its gradient, (3) the kinetic energy density, (4) the occupied molecular orbitals (MO), usually in form of Hartree-Fock exchange, and (5) the unoccupied or virtual MOs. GGA belongs to the second rung, while hybrid functionals belong to the fourth rung. At the fifth rung the inclusion of the virtual

orbitals allows for taking into account non-local, dynamical, electron correlation effects, that contribute to the long-range van der Waals (vdW) dispersion interactions. Many of the various functionals on the 5^{th} rung are based on either the random phase approximation (RPA) (Eshuis et al 2012; Paier et al 2012; Grimme and Steinmetz 2016) or second-order Møller-Plesset perturbation theory (MP2) (Grimme 2006; Goerigk and Grimme 2011), in the form of double hybrids (DH). Direct use of RPA and MP2 energies and variations thereof are also of interest for many applications. As a basic building block, the calculation of the RPA and MP2 energies have to be provided. We will in the subsequent sections concentrate on the theory and implementation of these methods.

2.1 Theory

We present briefly the theoretical framework of the methods and refer to the original works for more details. First, the resolution of the identity approximation for two electron repulsion integrals (ERIs) is introduced and then its application to the different correlation methods is formulated. The following index notation has been adopted: $i,j,k,\ldots$ refer to canonical occupied molecular orbitals (MOs), $a,b,c,\ldots$ to canonical virtual MOs, $\mu,\nu,\lambda,\ldots$ to atomic orbital basis set functions (AO), $P,Q,R,\ldots$ to auxiliary basis set functions (AUX). The one electron MO and AO functions are symbolized with ψ and ϕ, respectively. The number of occupied and virtual orbitals is denoted by o and v, while the total number of primary and auxiliary basis functions as n and N_a. In order to express, in general, the system size, the symbol N is used.

Periodic Boundary Conditions

In order to minimize boundary effects, simulations of condensed matter systems are performed using periodic boundary conditions. In periodic systems the infinite number of particles to be treated is reduced to the unique particles in the simulation cell and the calculation of the electronic energy involves an integration over the first Brillouin zone. For disordered systems, as for example liquids, this integration can be replaced by a single point in the center of the integration volume, the Γ-point. In the following chapters we will always assume that this Γ-point approximation is invoked and we can further assume that the single particle functions at this point are real.

The Resolution of the Identity (RI) Approximation

The two electron repulsion integrals (ERI), in Mulliken notation, of the type $(ia|jb)$ are of central importance for all the methods presented. Within the RI approx-

imation (Whitten 1973; Dunlap et al 1979), based on the Coulomb metric (Vahtras et al 1993), these integrals are factorized according to:

$$(ia|jb)_{RI} = \sum_{PQ}(ia|P)(P|Q)^{-1}(Q|jb) \tag{1}$$

where $(P|Q)^{-1}$ is the inverse matrix of the Coulomb metric,

$$(P|Q) = \iint \phi_P(\mathbf{r}_1)\frac{1}{|\mathbf{r}_1-\mathbf{r}_2|}\phi_Q(\mathbf{r}_2)d\mathbf{r}_1 d\mathbf{r}_2. \tag{2}$$

The auxiliary basis set size N_a grows only linearly with the system size (Feyereisen et al 1993). The main advantage of the RI approximation is that four center integrals of the type $(ia|jb)$ are computed from three and two center ERIs. This allows to strongly reduce the effort for the integral computation without significant loss of accuracy (Weigend and Häser 1997). Since the $(P|Q)$ matrix is positive definite its inverse can be efficiently obtained from a Cholesky decomposition

$$(P|Q) = \sum_R L_{PR}L^T_{RQ} \tag{3}$$

followed by inversion of the triangular matrix $\mathbf{L}$. In this way the factorization of the $(ia|jb)$ integrals can be expressed in a compact form as:

$$(ia|jb)_{RI} = \sum_P B^{ia}_P B^{jb}_P. \tag{4}$$

$\mathbf{B}$ is a matrix with ov rows and N_a columns, given by:

$$B^{ia}_P = \sum_R (ia|R)L^{-1}_{PR}. \tag{5}$$

Since the three center integrals $(ia|R)$ are computed starting from integrals over AOs $(\mu\nu|R)$, the final expression for the B^{ia}_P elements reads:

$$(ia|P) = \sum_\nu C_{\nu a}\sum_\mu C_{\mu i}\sum_R (\mu\nu|R)L^{-1}_{PR} \tag{6}$$

where $\mathbf{C}$ is the MO coefficient matrix.

Computation of the $\mathbf{B}$ matrix thus includes, first, calculation of $(P|Q)$ and via Cholesky decomposition and triangular inversion, $\mathbf{L}^{-1}$. Second, three center integrals $(\mu\nu|R)$ are computed and transformed using the $\mathbf{C}$ and $\mathbf{L}^{-1}$ matrices (Eqs. 6). The first two steps formally scale $O(N^2)$ and $O(N^3)$, respectively, while three center integral computation requires formally $O(N^3)$ operations and integral transformations scale $O(N^4)$. Within the RI approximation, the asymptotically dominating step in computing $\mathbf{B}$ is thus the index transformation.

RI-MP2 Method

In second order Møller-Plesset perturbation theory (Møller and Plesset 1934), the correlation energy $E^{(2)}$ for a closed shell system is given by:

$$E^{(2)} = -\sum_{i\leq j}^{o}(2-\delta_{ij})\sum_{ab}^{v}\frac{(ia|jb)[2(ia|jb)-(ib|ja)]}{\varepsilon_a+\varepsilon_b-\varepsilon_i-\varepsilon_j}. \tag{7}$$

where ε_a and ε_i are orbital energies. In a canonical MP2 energy algorithm the time limiting step is the computation of the $(ia|jb)$ integrals obtained from the ERIs over AO $(\mu\nu|\lambda\sigma)$ via four consecutive integral transformations. The computational effort for the first quarter transformation (no sparsity considered) is $O(on^4)$, making the MP2 energy calculation a method scaling as $O(N^5)$. The application of the RI approximation to MP2 is straightforward (Feyereisen et al 1993) and consists in replacing $(ia|jb)$ integrals with the approximated $(ia|jb)_{RI}$ given in Eq. 4. The computation of $(ia|jb)_{RI}$ requires $O(o^2v^2N_a)$ operations implying that the RI-MP2 method is also scaling $O(N^5)$. The main reason for the speed-up observed in RI-MP2 lies in the strongly reduced integral computation part.

RI Direct Random Phase Approximation Correlation Energy Method

The RPA correlation energy is given as the difference between the zero point energy of two harmonic oscillator excitation problems for which the first includes a correlated ground state (RPA) and the second not (configuration interaction singles) (Furche 2008; Scuseria et al 2008). Within the direct-RPA (dRPA) approach, which is RPA without exchange contributions (Eshuis et al 2010) E_c^{dRPA} can be expressed in terms of a frequency integral

$$E_c^{\mathrm{dRPA}} = \frac{1}{2}\int_{-\infty}^{+\infty}\frac{d\omega}{2\pi}\mathrm{Tr}(\ln(\mathbf{1}+\mathbf{Q}(\omega))-\mathbf{Q}(\omega)), \tag{8}$$

with the frequency dependent matrix $\mathbf{Q}(\omega)$ in the RI basis which is determined by

$$Q_{PQ}(\omega) = 2\sum_{i}^{o}\sum_{a}^{v}B_P^{ia}\frac{\varepsilon_a-\varepsilon_i}{\omega^2+(\varepsilon_a-\varepsilon_i)^2}B_Q^{ia}. \tag{9}$$

For a given ω, the computation of the integrand function in Eq. 8 using Eq. 9 requires $O(N^4)$ operations. The integral of Eq. 8 can be efficiently calculated by Clenshaw-Curtius numerical quadrature and usually $30-40$ quadrature points are enough to achieve micro-Hartree accuracy. Thus, the introduction of the resolution of the identity (RI) approximation and the frequency integration techniques for computing E_c^{dRPA} lead to a reduction of the computational cost to $O(N^4N_q)$ and $O(N^3)$ storage, where N_q is the number of quadrature points.

2.2 Nuclear gradients and stress tensor

Calculation of analytic derivatives is of central importance for applications in electronic structure theory. The specific derivatives needed for nuclear gradients and stress tensors have received most attention as they are connected to basic structure properties of molecules and materials. In almost all applications, the availability of analytic derivatives is of advantage for reasons of accuracy and efficiency. The quantum chemistry community has a long tradition in developing algorithms for analytic derivatives, especially also for non-variational methods as the ones considered here (Handy and Schaefer 1984). These techniques have been used to derive derivatives for double-hybrid functionals (Neese et al 2007) and RPA methods (Burow et al 2014). For periodic systems, derivatives for MP2 in the restricted (Del Ben et al 2015a) and unrestricted (Rybkin and VandeVondele 2016), as well as RPA (Ramberger et al 2017) methods have been reported.

Analytic derivatives for RI-MP2

The analytic derivative of the RI-MP2 energy $E_{\mathrm{RI}}^{(2)}$ with respect to a perturbation parameter x, for a closed-shell restricted Hartree-Fock wave function, is given by (Weigend and Häser 1997):

$$E_{\mathrm{RI}}^{(2)x} = \frac{dE_{\mathrm{RI}}^{(2)}}{dx} = 4\sum_{Q}^{\mathrm{AUX}}\sum_{\mu\nu}^{\mathrm{AO}}\Gamma_{\mu\nu}^{Q}(\mu\nu|Q)^{x} - 2\sum_{PQ}^{\mathrm{AUX}}\Gamma^{PQ}(P|Q)^{x} + 2\sum_{pq}^{\mathrm{MO}}\left[P_{pq}^{(2)}F_{pq}^{(x)} - W_{pq}^{(2)}S_{pq}^{(x)}\right]. \tag{10}$$

In the above expression, for each summation, a common structure can be recognized, that is the contraction of terms involving AO derivatives $(\mu\nu|Q)^{x}, (P|Q)^{x}, F_{pq}^{(x)}, S_{pq}^{(x)}$, with elements of the intermediates $\Gamma_{\mu\nu}^{Q}, \Gamma^{PQ}, P_{pq}^{(2)}, W_{pq}^{(2)}$. The first two summations involve the contraction of 3- and 2-center RI integral derivatives $(\mu\nu|Q)^{x}, (P|Q)^{x}$ with corrections to the 2-particle density matrix (2-PDM), $\Gamma_{\mu\nu}^{Q}$ and Γ^{PQ}. These quantities are available from the energy calculation (Del Ben et al 2015a). The last summation in Eq. 10 consists in the contraction of $P_{pq}^{(2)}$, the MP2 correction to the 1-PDM, and $W_{pq}^{(2)}$, the MP2 correction to the energy-weighted density matrix, with the skeleton derivatives of the Fock and overlap matrix elements

$$F_{pq}^{(x)} = \sum_{\mu\nu}^{\mathrm{AO}} C_{\mu p}\left[h_{\mu\nu}^{x} + \sum_{\lambda\sigma} P_{\lambda\sigma}^{\mathrm{HF}}(\mu\nu|\lambda\sigma)^{x} - \frac{1}{2}\sum_{\lambda\sigma} P_{\lambda\sigma}^{\mathrm{HF}}(\mu\lambda|\nu\sigma)^{x}\right] C_{\nu q} \tag{11}$$

$$S_{pq}^{(x)} = \sum_{\mu\nu}^{\mathrm{AO}} C_{\mu p} S_{\mu\nu}^{x} C_{\nu q}. \tag{12}$$

In Eq. 11, $h^x_{\mu\nu}$ and $(\mu\nu|\lambda\sigma)^x$ are the derivatives of the one-electron Hamiltonian integrals and the ERIs, while $P^{\mathrm{HF}}_{\mu\nu} = 2\sum_i^{occ} C_{\mu i}C_{\nu i}$ is the Hartree-Fock density matrix. In order to take advantage from sparsity, the update of the $E^{(2)}_{\mathrm{RI}}$ derivative is performed in the AO basis, after back transformation of $P^{(2)}_{pq}$ and $W^{(2)}_{pq}$ from the MO basis.

The diagonal blocks of the 1-PDM $P^{(2)}_{pq}$, can be calculated again using quantities from the energy calculation. The virt-occ block of $P^{(2)}$ contains information related to the orbital relaxation caused by the perturbation x, *i.e.* first order response of the MO coefficients. It is computed as the solution of the Z-vector equations (Handy and Schaefer 1984)

$$\sum_a^{virt}\sum_i^{occ}\left[\delta_{ij}\delta_{ab}(\varepsilon_a-\varepsilon_i)+A_{aibj}\right]P^{(2)}_{ai} = -L_{bj} \tag{13}$$

where A_{aibj} is an element of the orbital Hessian matrix

$$A_{aibj} = 4(ai|bj) - (ab|ij) - (aj|bi), \tag{14}$$

and L is a specific RI-MP2 Lagrangian matrix given by:

$$L_{bj} = 2\sum_a^{virt}\sum_Q^{\mathrm{AUX}}(ba|Q)\Gamma^Q_{ja} - 2\sum_i^{occ}\sum_Q^{\mathrm{AUX}}(ij|Q)\Gamma^Q_{ib} + \sum_{ac}^{virt}P^{(2)}_{ac}A_{acbj} + \sum_{ik}^{occ}P^{(2)}_{ik}A_{ikbj}. \tag{15}$$

Due to the large size of the orbital Hessian matrix $\mathbf{A}$ ($ov \times ov$), the linear system of equation 13 is commonly solved by iterative techniques. Rather than calculating and storing the full $\mathbf{A}$, at each iteration, the matrix-vector product $\sum_{ia}X_{ai}A_{aibj}$ is computed, with $\mathbf{X}$ being a trial solution. Finally, the MP2 correction to the energy-weighted density matrix $W^{(2)}_{pq}$ can be calculated from the relaxed 1-PDM $P^{(2)}_{pq}$. The methodology presented is of general validity for any perturbation parameter x. In particular, for the calculation of the forces acting on the ions, the gradients of $E^{(2)}_{\mathrm{RI}}$ with respect to the atomic positions have to be computed.

The RI-MP2 contribution to the total stress tensor is calculated according to (Nielsen and Martin 1985; Del Ben et al 2015a):

$$\Pi^{(2)}_{\alpha\beta} = -\frac{1}{3V}\sum_{\gamma=1}^{3}\frac{\partial E^{(2)}_{\mathrm{RI}}}{\partial h_{\alpha\gamma}}h^T_{\gamma\beta} \tag{16}$$

where $h_{\alpha\gamma}$ are elements of the matrix of the cell vectors (Bravais lattice vectors) given by a_1, a_2 and a_3, that is $\mathbf{h} = [a_1, a_2, a_3]$.

2.3 Implementation and performance

RI Gaussian and Plane-Waves Method

The Gaussian and Plane-Waves (GPW) method has been shown to be an efficient approach for computing ERIs especially when periodic boundary conditions are considered (Del Ben et al 2012). The basis of the GPW approach for computation of the ERIs is the direct formulation of the half transformed integrals of the type $(ia|\lambda\sigma)$ in term of the electrostatic potential v^{ia} of the pair density ρ^{ia}

$$\begin{aligned}(ia|\lambda\sigma) &= \iint \psi_i(\mathbf{r}_1)\psi_a(\mathbf{r}_1)\frac{1}{\mathbf{r}_{12}}\phi_\lambda(\mathbf{r}_2)\phi_\sigma(\mathbf{r}_2)d\mathbf{r}_1 d\mathbf{r}_2 \\ &= \int\left[\int\frac{\rho^{ia}(\mathbf{r}_1)}{\mathbf{r}_{12}}d\mathbf{r}_1\right]\phi_\lambda(\mathbf{r}_2)\phi_\sigma(\mathbf{r}_2)d\mathbf{r}_2 \\ &= \int v^{ia}(\mathbf{r}_2)\phi_\lambda(\mathbf{r}_2)\phi_\sigma(\mathbf{r}_2)d\mathbf{r}_2. \end{aligned} \tag{17}$$

The form of the last equation is essentially identical to the one used in the GPW method (Lippert et al 1997) to compute matrix elements of the Hartree potential. Thus, the highly efficient implementation of that operation in the CP2K code can be directly used and we refer to VandeVondele et al (2005a) for a detailed discussion.

Within the RI approximation, two types of ERIs have to be computed, the two center $(P|Q)$ and three center $(ia|P)$ integrals. Three center integrals are computed starting from the integrals over AOs that are subsequently transformed with $\mathbf{C}$ and $\mathbf{L^{-1}}$. The index transformation over the auxiliary basis can be avoided, since it is possible to directly compute half transformed integrals for an associated density ρ as

$$\begin{aligned}(\mu\nu|P) = \sum_R(\mu\nu|R)L^{-1}_{PR} &= \iint\phi_\mu(\mathbf{r}_1)\phi_\nu(\mathbf{r}_1)\frac{1}{\mathbf{r}_{12}}\left[\sum_R\phi_R(\mathbf{r}_2)L^{-1}_{PR}\right]d\mathbf{r}_1 d\mathbf{r}_2 \\ &= \int\phi_\mu(\mathbf{r}_1)\phi_\nu(\mathbf{r}_1)\left[\int\frac{\rho^P(\mathbf{r}_2)}{\mathbf{r}_{12}}d\mathbf{r}_2\right]d\mathbf{r}_1 = \int\phi_\mu(\mathbf{r}_1)\phi_\nu(\mathbf{r}_1)v^P(\mathbf{r}_1)d\mathbf{r}_1. \end{aligned} \tag{18}$$

The same approach holds for the $(P|Q)$ integrals. An alternative way to calculate these integrals over Gaussian basis functions using analytic Ewald techniques is also available (Wilhelm et al 2016).

Of central importance in GPW is the representation of the density on a regular grid, which is equivalent to an expansion of the density in an auxiliary basis of plane waves (PW). The expansion is given by

$$\rho^P(\mathbf{r}) \approx \frac{1}{\Omega}\sum_{|\mathbf{G}|\le G_c}\rho^P(\mathbf{G})e^{i\mathbf{G}\cdot\mathbf{r}} \tag{19}$$

where the sum over the reciprocal lattice vectors $\mathbf{G}$ is determined by the resolution of the grid. $\rho^P(\mathbf{G})$ are the Fourier coefficients of the density, and Ω is the volume of the

simulation cell. Fast Fourier transforms (FFTs) efficiently change between real space and reciprocal space representations. In reciprocal space, it becomes straightforward to solve the Poisson equation for the potential v^P

$$v^P(\mathbf{G}) = \frac{4\pi}{G^2}\rho^P(\mathbf{G}) \tag{20}$$

and an additional back FFT will yield the potential in real space. For $\mathbf{G} = 0$ the value of the potential is set to zero, corresponding to a constant shift of the potential, enforcing zero average. Due to the orthogonality of the occupied-virtual orbitals this shift has no influence on the final value of the $(ia|P)$ integrals. Within the GPW method pseudopotentials have to be employed in order to have sufficiently smooth densities. Once the potential v^P is available, the numerical integration over the basis functions is performed by summing over the grid points. For a given $|P)$, all matrix elements that are non-zero within a given threshold can be obtained in linear scaling time. A further gain in efficiency is obtained by employing a multi-grid technique that represents the potential v^P on grids with increasingly coarser grid spacing. Finally, $(\mu\nu|P)$ integrals are transformed into MO ERIs using (sparse) matrix multiplication as implemented in the DBCSR library (Borštnik et al 2014).

The accuracy of the RI approximation is directly related to the completeness of the auxiliary basis set. It has been shown, that it is possible to generate compact auxiliary basis sets with a size of approximately three times the size of the orbital basis set, that have a transferable overall accuracy of $\approx$ 1mHartree/atom (Weigend et al 1998). Specific RI basis sets for the application in condensed systems have been generated and tested (Del Ben et al 2013a).

	cc-TZ	cc-QZ	aug-cc-TZ
MAD	0.43	0.27	0.15
RMSD	0.52	0.31	0.21
Max	1.24	0.71	0.59
MA%D	7.45	5.42	3.48

Table 1: Counter-Poise corrected PWPB95-D3 interaction energies (kcal/mol) of the S22 set obtained employing the cc-TZ, cc-QZ and aug-cc-TZ basis sets (Del Ben et al 2013a). Mean absolute deviation (MAD), root mean square deviation (RMSD), maximum deviation (Max) and mean absolute percentage deviation (MA%D) of each basis set with respect to the reference values (Goerigk and Grimme 2011) are reported.

The setup used in the applications presented later, has been tested with respect to the basis set error for correlated calculations. The slow convergence of correlated methods with basis set size is a well studied problem in quantum chemistry. In table 1 results for three basis sets are presented for calculations of the S22 reference sets

using a double-hybrid functional. An improvement of results with the increase of the basis set can be observed. However, it should be noted that the reference used is itself not fully converged and that there are other parameters, e.g. the pseudopotential used, that result in differences. It can be seen that the results obtained with the cc-TZ basis, that is used in the liquid water simulations, is of good quality, but cannot be considered fully converged.

Parallel Implementation of the RI-GPW methods

In this section the parallelization strategies for the methods introduced are presented. The algorithms are split in two steps, the first deals with the computation of the ERIs $(ia|P)$, and is common for all methods, the second is specific to the type of correlation energy calculated. The parallelization is achieved with a multi-level hybrid OpenMP/MPI scheme using a careful process layout. The first level of parallelization corresponds to distributing the work performed for a single given auxiliary basis function ϕ_P or vector $|P) = \sum_R \phi_R L^{-1}_{PR}$. The second level of parallelization corresponds to a distribution of these nearly independent calculations. The N_p processes available in total are split in N_G groups, each group working on a given ϕ_P or $|P)$ and each consisting of N_w processes ($N_p = N_G N_w$). The first level of parallelization involves parallel FFTs, halo-exchanges, and sparse matrix multiplications over N_w processes and corresponds to the standard parallelization scheme for DFT calculations in CP2K (VandeVondele et al 2005a). The second level is straightforward and only requires inter-group redistribution of two center ERIs $(Q|P)$ in order to calculate $\mathbf{L}^{-1}$.

The total work load for the integral computation is distributed by splitting the auxiliary basis functions into N_G ranges. Additionally, each of the N_w processes within a group is assigned a range of virtual orbital indices, while the occupied orbital index is fully replicated. Once the integrals $(ia|P)$ are available we can proceed to calculate the RI-MP2 energy. Since N_w is usually small compared to the total number of processes, the virtual index a is distributed over a small number of MPI tasks within the group G while the auxiliary index P is distributed over a large number of N_G groups. First, the independent ij pairs ($i \leq j$) are distributed over the N_G groups. For each ij pair, the full range of the auxiliary index P is collected on a local buffer from all other groups, while keeping the virtual index distribution within the group. The $(ia|jb)$ integrals are generated for the actual ij pair in a matrix-multiplication fashion (Eq. 4) requiring only a small amount of communication within the group. Once the $(ia|jb)$ are available, they are accumulated into the MP2 energy according to Eq. 7, requiring an additional negligible amount of communication within the group. With this choice, the main source of inter-group communication in the parallel algorithm is related to the redistribution of the B^P_{ia} integrals, required for each ij pair. The time determining step is the $(ia|jb)$ integral generation that is essentially a local matrix multiplication. This allows to fully exploit the performance of highly optimized routines and can be further accelerated by employing a hybrid implementation that utilizes graphics processing units (GPUs).

The dRPA correlation energy implementation is based on the method developed by Del Ben et al (2013a). The parallel algorithm has a two level work load distribution. The first level corresponds to the distribution of the work necessary for a given quadrature point of the integral in Eq. 8. The second level distributes the calculation of the independent quadrature points over subgroups of processes. The **B** matrix has to be replicated within the groups in order for the algorithm to proceed independently for each integration point. As a first task the matrix $\mathbf{B}'$ is calculated as $\mathbf{G}(\omega)\mathbf{B}$. Since $\mathbf{G}(\omega)$ is a $ov \times ov$ diagonal matrix with elements $G_{ia,ia}(\omega) = (\varepsilon_a - \varepsilon_i)((\varepsilon_a - \varepsilon_i)^2 + \omega^2)^{-1}$ the calculation of $\mathbf{B}'$ proceeds without communication. The time determining step of the algorithm is the calculation of the matrix $\mathbf{Q}(\omega)$ computed as $2\mathbf{B}^{\mathbf{T}}\mathbf{B}'(\omega)$. This task is performed as a standard parallel matrix multiplication. The calculation of $\mathrm{Tr}[\ln(\mathbf{Q}(\omega)+\mathbf{1})]$ can be efficiently carried out by considering the identity $\mathrm{Tr}[\ln \mathbf{A}] = \ln(\mathrm{Det}[\mathbf{A}])$, that is:

$$\mathrm{Tr}[\ln(\mathbf{Q}(\omega)+\mathbf{1})] = 2\sum_{i=1}^{N_a} \ln(U_{ii}) \tag{21}$$

where the **U** matrix is the Cholesky decomposition of $\mathbf{Q}(\omega)+\mathbf{1}$.

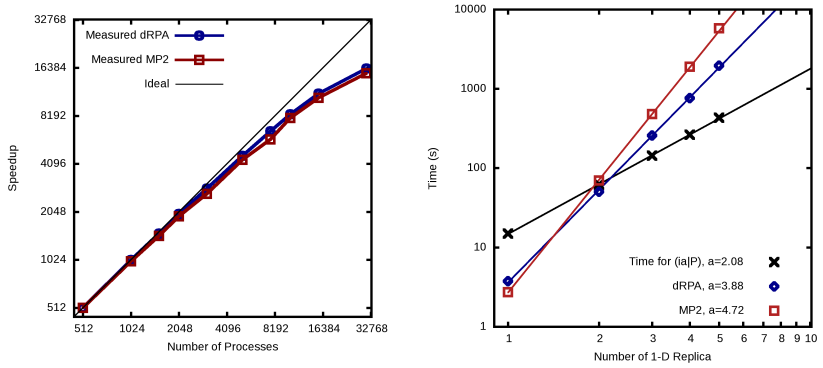

(a) (b)

Fig. 1: (a) Measured speed up with respect to 512 processes for the calculation of the MP2 and dRPA energy of 64 bulk water molecules. dRPA calculation performed employing 60 quadrature points for the numerical integration. (b) CPU time as a function of the number of replicas of the supercell containing 32 H_2O molecules. 20 quadrature points were used for dRPA. Lines represent a linear two-parameter fit of the form $y = bx^a$.

The excellent performance of the presented implementation can be seen from the results in figure 1. Panel a shows the achieved scaling for a 64 water molecule system using a range of 512 to 32768 processes. Both methods, MP2 and dRPA, show similar overall scalability with $\approx 80\%$ efficiency over the full range tested. In

panel b timings for the RI integral generation as well as the energy calculation for different methods is shown. In a doubly logarithmic plot the system size (generated as increasing water systems) is given versus the total CPU time. All measured timings show a linear dependency, resulting in an estimate for the true scaling of the method from the observed slope of the linear fit. The observed scaling laws closely reproduce the theoretical scaling from the analysis of the implemented algorithms.

3 Application: Properties of Water

Despite the apparent simplicity of the H_2O molecule, bulk liquid water has a rich chemistry and physics. This is commonly illustrated referring to its many anomalous properties. These macroscopic properties are well characterized experimentally, but resolving the underlying atomistic picture is far more difficult (Errington and Debenedetti 2001), and even the structure of the neat liquid is still debated intensely (Nilsson and Pettersson 2011; Soper 2013). Ultimately, our understanding must go beyond the neat liquid. The properties of water, as a solvent or reactant, in the bulk, near interfaces or in confinement is of central importance in many fields, such as biology, electrochemistry, catalysis, and earth and climate science.

Theory and simulation can complement the experimental efforts, and have a long tradition. For example, liquid water was among the first systems studied when molecular dynamics (MD) based on empirical potentials became available in the 1970s (Rahman and Stillinger 1971). Recent models are mostly derived based on high level electronic structure calculation, and show excellent agreement with experiment for a variety of properties at low computational cost. However, empirical methods might fail when applied outside their fitting range, and the effort to parameterize the models and refine the employed functional forms cannot be underestimated. This challenge rises considerably as soon solutes come into play, or if more complicated chemical phenomena, such as autodissociation and reactivity, must be taken into account. Computing the intermolecular interactions during the entire simulation using electronic structure theory is an alternative to empirical models as complexity increases, since no assumptions on the form of the interactions must be made. The pioneering application of electronic structure theory to bulk liquid water was based on Kohn–Sham density functional theory using a GGA density functional approximation (Laasonen et al 1993), and the same class of functionals has been employed for most subsequent applications, see e.g. VandeVondele et al (2005b); McGrath et al (2005b). Recently, also hybrid functionals have been used for the simulation of liquid water (Todorova et al 2006; Guidon et al 2008; DiStasio et al 2014). The importance of vdW interactions for the description of liquid water has also become apparent and current applications rely on different available approaches to augment standard local functionals. The two main of these approaches, empirical pair potentials (Grimme et al 2010) and explicit non-local correlation functionals (Dion et al 2004) are outside the Perdew classification. The performance of these approaches have been extensively

tested and results show a systematic improvement upon the uncorrected GGA or hybrid functionals (Schmidt et al 2009; DiStasio et al 2014).

We assess the performance of various methods, with a focus on MP2, RPA, and double hybrid functionals. In particular, the structural and dynamical properties of bulk liquid water have been studied by means of Monte Carlo (MC) and Molecular Dynamics (MD) simulations (Del Ben et al 2013b, 2015b). The MC simulations have been performed in the NpT ensemble under ambient pressure and temperature and are focused on the structural properties, while MD has been employed to obtain dynamical observables namely the infrared spectrum and the diffusion constant (Del Ben et al 2015b). A significant advantage of the MC scheme is that the sampling of the phase space is solely determined by a total energy based criterion, and that forces and stresses are not explicitly required, simplifying the implementation. The downside is that dynamical properties are not available, and that suitable moves are needed to efficiently explore large portions of the configuration space.

Computational Setup

All calculations presented have been performed with the CP2K program. Th CP2K code makes use of a dual representation for the electronic density and MO's in terms of Gaussian and Plane-Wave (GPW) (Lippert et al 1997; VandeVondele et al 2005a). Unless specified otherwise, the Gaussian basis is of correlation consistent triple zeta quality (Dunning 1989; Del Ben et al 2012), while the PW cutoff is set to 800 Ry. To efficiently expand the density and orbitals in plane waves within GPW, core electrons are replaced by pseudopotentials (Goedecker et al 1996), that have been parametrized for the employed functionals. The exact exchange calculations are performed employing a Γ-point implementation making use of a truncated Coulomb operator to avoid divergence of the energy (Guidon et al 2008, 2009), the truncation radius is set to 6 Å. The RI auxiliary basis is specifically fitted for this purpose (Del Ben et al 2015b). All dRPA calculations have been performed employing KS Perdew-Burke-Ernzerhof (PBE) (Perdew et al 1996) orbitals as input. More details on the computational setups are reported in supporting information of Del Ben et al (2015b). The model system is made of 64 H_2O molecules in a cubic box under periodic boundary conditions (PBC). The Monte Carlo simulations have been performed with thermodynamic constraints set to ambient conditions, that is, $T = 295$K and $p = 1$bar. The MC efficiency is improved with the presampling of moves (Iftimie et al 2000), in the actual case, the approximated potential is calculated at the DFT level employing the PBE1W (García-González et al 2007) functional, for which the basis and D3 parameters have been specifically refitted in order to closely approximate the energy of the wavefunction methods, and thus to increase acceptance of moves. Molecular dynamics (MD) simulations where started from equilibrated MC configurations and used a multiple timestep scheme, previously proposed in the context of hybrid density functionals (Guidon et al 2008).

Structural Properties of Liquid Water

In figure 2 the density fluctuation over the MC trajectory obtained with the MP2 and RPA methods are reported. At the RPA level, the density quickly equilibrates, giving an average density of 0.994 g/mL in excellent agreement with experiment. The root mean square deviations of the instantaneous density is 0.015 g/mL similarly to that of the MP2 method which has an average density of 1.020 g/mL. As RPA is computationally less demanding than MP2, roughly twice the number of MC cycles have been performed relative to MP2 (26.8 kcycles vs. 14.6 kcycles). Nevertheless, finite sampling times cannot exclude sudden structural rearrangements on longer timescales. This was observed at the PWPB95-D3 level (Del Ben et al 2015b), where initially, the fluctuations of the instantaneous density seem to equilibrate to a stable average value of 1.002 g/mL. However, later a sharp transition occurred to a high density phase, which was not fully stabilized after an additional 10000 cycles. Fluctuations between high density (HD) and low density (LD) phases would be expected near a liquid-liquid phase transition, for small samples, but the high computational cost of these simulations did not allow for exploring this in depth. Overall the results support the view that the MP2 and RPA methods describe the potential energy surface of bulk liquid water accurately, and emphasizes the value of treating dispersion interactions at the same level as hydrogen bond interactions.

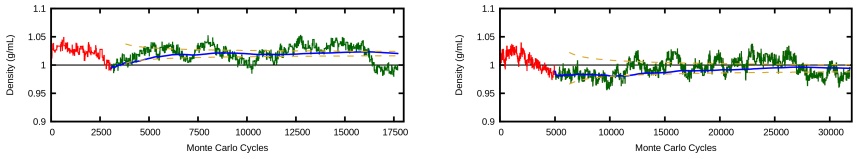

(a) (b)

Fig. 2: The red portion of the plots denotes MC cycles considered for equilibration, the green parts refers to that used for the calculation of the average properties, the blue line shows the running average density. Estimated errors are reported as yellow dashed lines. Panel (a) shows results for MP2, panel (b) for RPA.

Figure 3 shows the radial distribution functions (RDF) obtained at the MP2 and RPA level, respectively. The RDFs are in very good agreement with the recent experimental $g_{OO}(r)$ obtained from X-ray diffraction (Skinner et al 2013). The height of the first peak is overestimated by about 10%, while the features of the long range part are remarkably well reproduced, being only very slightly more structured. In order to gain additional information on the local environment around each water molecule in the liquid, the positions of the 4^{th} and 5^{th} neighboring H_2O were analyzed, as they serve as an indicator for the overlap of coordination shells. GGAs and hybrid functionals not corrected for van der Waals interactions give highly structured and significantly less dense (around 10-20%) liquids. The introduction of dispersion improves the liquid description, but in general gives too dense water

(5-10%) (Del Ben et al 2015b). In particular the distributions of the 4^{th} and 5^{th} neighboring waters show a clear separation between the first and second coordination shells for GGA functionals, whereas they move closer when vdW interactions are included, and a similar overlapping pattern is found for MP2 and RPA methods.

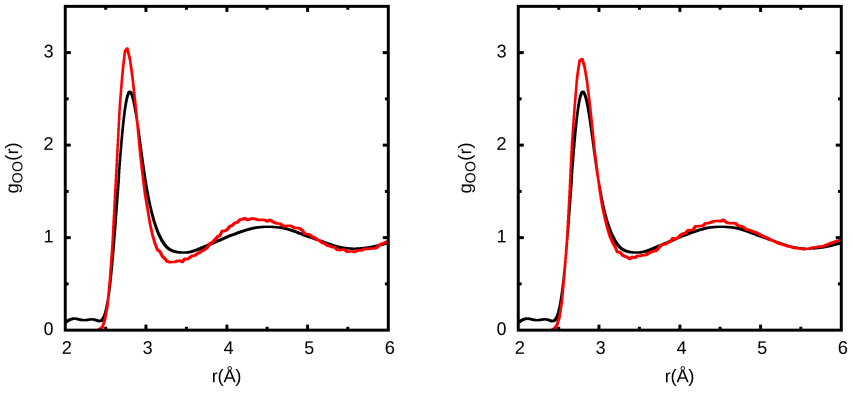

Fig. 3: Oxygen-Oxygen pair radial distribution functions as obtained from the NpT-MC simulations ($T = 295$ K and $p = 1$ bar) at (a) MP2 (b) RPA level of theory (solid red line). Experimental RDF (solid black line) taken from Skinner et al (2013).

The accurate prediction of the water density and structure requires thus a balance between vdW and hydrogen bond interactions. On this basis, it can be argued that the accurate prediction of the water density and structure by RPA and MP2 can be attributed to the fact that these theories provide, for this system, a correct balance between hydrogen-bond and van der Waals interactions. Reaching this balance might be facilitated by the fact that both interactions are obtained from the same level of theory. Note that in general, MP2 and RPA tend to overbind respectively underbind noncovalent complexes as e.g. found in the S22 set (Jurecka et al 2006), which covers a broader range of systems, including compounds that are aromatic or have double bonds (Eshuis and Furche 2012; Ren et al 2012). While these effects are not pronounced for water, it might nevertheless lead to the slightly higher and lower water densities calculated at the MP2 and RPA level, respectively.

To put these results in context, table 2 summarizes the density and structural features of the RDF of liquid water obtained from NpT-MC simulations at different level of theory, but with consistent choice of simulation parameters (Del Ben et al 2015b). In addition to functionals including orbital correlation (RPA, MP2), standard GGA and hybrid functionals (PBE, PBE0) with D3 and non-local vdW corrections are shown. The reported average values show the slight overestimation when GGA and hybrid functionals with the D3 vdW corrections are used. For the considered non-local van der Waals functional the obtained results show a larger density of

	Density [g/mL]		1^{st} Max		1^{st} Min		2^{nd} Max	
	ρ	Δ_ρ	r[Å]	$g_{OO}(r)$	r[Å]	$g_{OO}(r)$	r[Å]	$g_{OO}(r)$
PBE-D3	1.055	0.006	2.73	3.07	3.25	0.69	4.43	1.21
PBE0-D3	1.053	0.005	2.74	2.88	3.29	0.79	4.32	1.21
optB88-vdW	1.081	0.003	2.74	2.94	3.34	0.80	4.31	1.21
MP2	1.020	0.004	2.76	3.05	3.32	0.72	4.41	1.21
RPA	0.994	0.006	2.78	2.93	3.41	0.78	4.49	1.19
exp.	1.00		2.80	2.57	3.45	0.84	4.5	1.12

Table 2: Average Density and structural data obtained from the NpT-MC simulations ($T = 295$K and $p = 1$bar). The method labeled with optB88-vdW (Klimeš et al 2010, 2011) represents a functional of the non-local van der Waals type. The label D3 stands for a dispersion correction according to Grimme et al (2010). For the calculated average densities an error estimation is reported (Δ_ρ).

$\sim$8%, and the structure of the liquid is rather well reproduced but with all features shifted to shorter distances, in agreement with previous NVT simulations (Wang et al 2011). Even though at the limit of statistical accuracy, both the inclusion of the D3 correction and the use of hybrid functionals reduces the height of the first peak of the $g_{OO}(r)$ for PBE. This combined effect of dispersion and exchange has been emphasized recently (DiStasio et al 2014).

GGA functionals, which underestimate the band gap, lead to a too polarizable solvent, which in turn should lead to too strong hydrogen bonds. This is similar to the effect of charge transfer from anions to the solvent that has been observed to be too strong for GGAs as compared to hybrids (VandeVondele et al 2012). The effect of hybrid functionals on the dielectric constant of water ice has been quantified (Schönherr et al 2014) showing that GGA functionals lead to more polar structures while also overestimating the polarization of these structures. Whereas the effect of band gap underestimation is already noticeable in neat water, it becomes even more visible in the context of aqueous electrochemistry. Redox levels of various species can be significantly influenced, if water band edges are incorrect, in particular they will be pushed up if these are close to the valence band of the liquid (Adriaanse et al 2012). Results obtained with RPA and double hybrid functionals for redox levels near the band edges appear promising (Cheng and VandeVondele 2016). This highlights the importance of going beyond the neat liquid in assessing the performance of electronic structure theory for liquid water.

Finally the equilibrium parameters of ice I*h*, calculated at various level of theory, and reported in table 3 for comparison (Del Ben et al 2015b). The results reported are obtained at 0K neglecting nuclear quantum effects and zero point energies. Despite important in many situations, these effects have been shown to have a lesser influence $(\leq 1\%)$ for the equilibrium volume of ice I*h* both theoretically (Santra et al 2013; Pamuk et al 2012) and experimentally (Röttger et al 2012). Analogously to the

	E_{coh} [kJ/mol]	V_{mol} [Å^3]	ρ [g/mL]
PBE	-62.8	30.69	0.975
MP2	-58.7	31.34	0.955
RPA	-52.5	32.37	0.924
exp.	-58.9	32.05	0.933

Table 3: Equilibrium volumes and energies (at 0 K) for ice I*h* expressed per molecule without corrections for the quantum nature of the nuclei and zero point energies. Experimental values are from Hobbs (1974); Whalley (1984).

liquid water case, the calculated ice densities are $\sim$2% larger and $\sim$1% smaller than experimental results for MP2 and RPA respectively. At both the MP2 and RPA level, these results show the non-trivial prediction that ice floats on water, with a quantitatively correct ratio of liquid and solid density.

4 Outlook

With the methods described here, nonlocal wavefunction correlation methods can be applied to liquids, solutions, crystals, and simple interfaces. As the available computational resources continue to grow, such applications will become increasingly more routine. At the same time, the algorithms will be further refined and improved. Reduced scaling algorithms (Wilhelm et al 2016) will make it possible to tackle larger systems. Multiple timestep algorithms are developed, that make ab initio molecular dynamics simulations using high level methods more efficient. These methods are also combined with path integral techniques (Kapil et al 2016) and bring simulations including nuclear quantum effects within reach.

Acknowledgements This research was partly supported by NCCR MARVEL, funded by the Swiss National Science Foundation. We acknowledge that the results of this research have been achieved using the PRACE Research Infrastructure resource Hermit based in Germany at Stuttgart (HLRS). Additional calculations were enabled by the Swiss National Supercomputer Centre (CSCS).

References

Adriaanse C, Cheng J, Chau V, Sulpizi M, VandeVondele J, Sprik M (2012) Aqueous Redox Chemistry and the Electronic Band Structure of Liquid Water. J Phys Chem Lett 3:3411–3415

Borštnik U, VandeVondele J, Weber V, Hutter J (2014) Sparse matrix multiplication: The distributed block-compressed sparse row library. Parallel Comput 40:47–58

Burow AM, Bates JE, Furche F, Eshuis H (2014) Analytical First-Order Molecular Properties and Forces within the Adiabatic Connection Random Phase Approximation. J Chem Theory Comput

10:180–194
Car R, Parrinello M (1985) Unified Approach for Molecular Dynamics and Density–Functional Theory. Phys Rev Lett 55:2471–2474
Cheng J, VandeVondele J (2016) Calculation of Electrochemical Energy Levels in Water Using the Random Phase Approximation and a Double Hybrid Functional. Phys Rev Lett 116:086,402
Del Ben M, Hutter J, VandeVondele J (2012) Second-Order Møller–Plesset Perturbation Theory in the Condensed Phase: An Efficient and Massively Parallel Gaussian and Plane Waves Approach. J Chem Theory Comput 8:4177–4188
Del Ben M, Hutter J, VandeVondele J (2013a) Electron Correlation in the Condensed Phase from a Resolution of Identity Approach Based on the Gaussian and Plane Waves Scheme. J Chem Theory Comput 9:2654–2671
Del Ben M, Schönherr M, Hutter J, VandeVondele J (2013b) Bulk Liquid Water at Ambient Temperature and Pressure from MP2 Theory. J Phys Chem Lett 4:3753–3759
Del Ben M, Hutter J, VandeVondele J (2015a) Forces and stress in second order Møller-Plesset perturbation theory for condensed phase systems within the resolution-of-identity Gaussian and plane waves approach. J Chem Phys 143:102,803
Del Ben M, Hutter J, VandeVondele J (2015b) Probing the structural and dynamical properties of liquid water with models including non-local electron correlation. J Chem Phys 143:054,506
Dion M, Rydberg H, Schröder E, Langreth DC, Lundqvist BI (2004) Van der Waals Density Functional for General Geometries. Phys Rev Lett 92:246,401
DiStasio RA, Santra B, Li Z, Wu X, Car R (2014) The individual and collective effects of exact exchange and dispersion interactions on the ab initio structure of liquid water. J Chem Phys 141:084,502
Dunlap BI, Connolly JWD, Sabin JR (1979) On some approximations in applications of X alpha theory. J Chem Phys 71:3396–3402
Dunning TH (1989) Gaussian basis sets for use in correlated molecular calculations. I. The atoms boron through neon and hydrogen. J Chem Phys 90:1007–1023
Errington JR, Debenedetti PG (2001) Relationship between structural order and the anomalies of liquid water. Nature 409:318–321
Eshuis H, Furche F (2012) Basis set convergence of molecular correlation energy differences within the random phase approximation. J Chem Phys 136:084,105
Eshuis H, Yarkony J, Furche F (2010) Fast computation of molecular random phase approximation correlation energies using resolution of the identity and imaginary frequency integration. J Chem Phys 132:234,114
Eshuis H, Bates J, Furche F (2012) Electron correlation methods based on the random phase approximation. Theor Chem Acc 131:1084
Feyereisen M, Fitzgerald G, Komornicki A (1993) Use of approximate integrals in ab initio theory. An application in MP2 energy calculations. Chem Phys Lett 208:359–363
Furche F (2008) Developing the random phase approximation into a practical post-Kohn–Sham correlation model. J Chem Phys 129:114,105
García-González P, Fernández JJ, Marini A, Rubio A (2007) Advanced Correlation Functionals: Application to Bulk Materials and Localized Systems. J Phys Chem A 111:12,458–12,465
Goedecker S, Teter M, Hutter J (1996) Separable dual-space Gaussian pseudopotentials. Phys Rev B 54:1703–1710
Goerigk L, Grimme S (2011) Efficient and Accurate Double-Hybrid-Meta-GGA Density Functionals: Evaluation with the Extended GMTKN30 Database for General Main Group Thermochemistry, Kinetics, and Noncovalent Interactions. J Chem Theory Comput 7:291–309
Grimme S (2006) Semiempirical hybrid density functional with perturbative second-order correlation. J Chem Phys 124:034,108
Grimme S, Steinmetz M (2016) A computationally efficient double hybrid density functional based on the random phase approximation. Phys Chem Chem Phys 18:20,926–20,937
Grimme S, Antony J, Ehrlich S, Krieg H (2010) A consistent and accurate ab initio parametrization of density functional dispersion correction (DFT-D) for the 94 elements H-Pu. J Chem Phys 132:154,104

Guidon M, Schiffmann F, Hutter J, VandeVondele J (2008) Ab initio molecular dynamics using hybrid density functionals. J Chem Phys 128:214,104

Guidon M, Hutter J, VandeVondele J (2009) Robust Periodic Hartree–Fock Exchange for Large-Scale Simulations Using Gaussian Basis Sets. J Chem Theory Comput 5:3010–3021

Handy NC, Schaefer HF (1984) On the evaluation of analytic energy derivatives for correlated wave functions. J Chem Phys 81:5031–5033

Hobbs P (1974) Ice Physics. Clarendon Press

Hutter J (2012) Car-Parrinello molecular dynamics. WIREs Comput Mol Sci 2:604–612

Iftimie R, Salahub D, Wei D, Schofield J (2000) Using a classical potential as an efficient importance function for sampling from an ab initio potential. J Chem Phys 113:4852–4862

Jurecka P, Sponer J, Cerny J, Hobza P (2006) Benchmark database of accurate (MP2 and CCSD(T) complete basis set limit) interaction energies of small model complexes, DNA base pairs, and amino acid pairs. Phys Chem Chem Phys 8:1985–1993

Kapil V, VandeVondele J, Ceriotti M (2016) Accurate molecular dynamics and nuclear quantum effects at low cost by multiple steps in real and imaginary time: Using density functional theory to accelerate wavefunction methods. J Chem Phys 144:054,111

Klimeš J, Bowler D, Michaelides A (2010) Chemical accuracy for the van der Waals density functional. J Phys: Condens Matter 22:022,201

Klimeš J, Bowler D, Michaelides A (2011) Van der Waals density functionals applied to solids. Phys Rev B 83:1–13

Laasonen K, Sprik M, Parrinello M, Car R (1993) “Ab Initio” Liquid Water. J Chem Phys 99:9080–9089

Lippert G, Hutter J, Parrinello M (1997) A hybrid Gaussian and plane wave density functional scheme. Mol Phys 92:477–488

Marx D, Hutter J (2009) Ab Initio Molecular Dynamics: Basic Theory and Advanced Methods. Cambridge University Press

McGrath MJ, Siepmann JI, Kuo IFW, Mundy CJ, VandeVondele J, Hutter J, Mohamed F, Krack M (2005a) Isobaric-Isothermal Monte Carlo Simulations from First Principles: Application to Liquid Water at Ambient Conditions. ChemPhysChem 6:1894–1901

McGrath MJ, Siepmann JI, Kuo IFW, Mundy CJ, VandeVondele J, Sprik M, Hutter J, Mohamed F, Krack M, Parrinello M (2005b) Toward a Monte Carlo program for simulating vapor-liquid phase equilibria from first principles. Comput Phys Comm 169:289 – 294

Møller C, Plesset MS (1934) Note on an Approximation Treatment for Many-Electron Systems. Phys Rev 46:618–622

Neese F, Schwabe T, Grimme S (2007) Analytic derivatives for perturbatively corrected ”double hybrid” density functionals: Theory, implementation, and applications. J Chem Phys 126:124,115

Nielsen OH, Martin RM (1985) Quantum-mechanical theory of stress and force. Phys Rev B 32:3780–3791

Nilsson A, Pettersson L (2011) Perspective on the structure of liquid water. Chemical Physics 389:1 – 34

Paier J, Ren X, Rinke P, Scuseria GE, Grüneis A, Kresse G, Scheffler M (2012) Assessment of correlation energies based on the random-phase approximation. New J Phys 14:043,002

Pamuk B, Soler JM, Ramírez R, Herrero CP, Stephens PW, Allen PB, Fernández-Serra MV (2012) Anomalous Nuclear Quantum Effects in Ice. Phys Rev Lett 108:193,003

Perdew JP, Burke K, Ernzerhof M (1996) Generalized Gradient Approximation Made Simple. Phys Rev Lett 77:3865–3868

Perdew JP, Ruzsinszky A, Tao J, Staroverov VN, Scuseria GE, Csonka GI (2005) Prescription for the design and selection of density functional approximations: More constraint satisfaction with fewer fits. J Chem Phys 123:062,201

Rahman A, Stillinger FH (1971) Molecular Dynamics Study of Liquid Water. J Chem Phys 55:3336–3359

Ramberger B, Schäfer T, Kresse G (2017) Analytic Interatomic Forces in the Random Phase Approximation. Phys Rev Lett 118:106,403

Ren X, Rinke P, Joas C, Scheffler M (2012) Random-phase approximation and its applications in computational chemistry and materials science. J Mater Sci 47:7447

Röttger K, Endriss A, Ihringer J, Doyle S, Kuhs WF (2012) Lattice constants and thermal expansion of H_2O and D_2O Ice I*h* between 10 and 265K. Addendum. Acta Crystallogr Sec B 68:91

Rybkin VV, VandeVondele J (2016) Spin-Unrestricted Second-Order Møller–Plesset (MP2) Forces for the Condensed Phase: From Molecular Radicals to F-Centers in Solids. J Chem Theory Comput 12:2214–2223

Santra B, Klimeš J, Tkatchenko A, Alfè D, Slater B, Michaelides A, Car R, Scheffler M (2013) On the accuracy of van der Waals inclusive density-functional theory exchange-correlation functionals for ice at ambient and high pressures. J Chem Phys 139:154,702

Schmidt J, VandeVondele J, Kuo IFW, Sebastiani D, Siepmann JI, Hutter J, Mundy CJ (2009) Isobaric–Isothermal Molecular Dynamics Simulations Utilizing Density Functional Theory: An Assessment of the Structure and Density of Water at Near–Ambient Conditions. J Phys Chem B 113:11,959–11,964

Schönherr M, Slater B, Hutter J, VandeVondele J (2014) Dielectric Properties of Water Ice, the Ice Ih/XI Phase Transition, and an Assessment of Density Functional Theory. J Phys Chem B 118:590–596

Scuseria GE, Henderson TM, Sorensen DC (2008) The ground state correlation energy of the random phase approximation from a ring coupled cluster doubles approach. J Chem Phys 129:231,101

Skinner LB, Huang C, Schlesinger D, Pettersson LGM, Nilsson A, Benmore CJ (2013) Benchmark oxygen-oxygen pair-distribution function of ambient water from x-ray diffraction measurements with a wide Q-range. J Chem Phys 138:074,506

Soper AK (2013) The Radial Distribution Functions of Water as Derived from Radiation Total Scattering Experiments: Is There Anything We Can Say for Sure? ISRN Physical Chemistry 2013:279,463

Todorova T, Seitsonen AP, Hutter J, Kuo IFW, Mundy CJ (2006) Molecular Dynamics Simulation of Liquid Water: Hybrid Density Functionals. J Phys Chem B 110:3685–3691

Vahtras O, Almlöf J, Feyereisen M (1993) Integral approximations for LCAO-SCF calculations. Chem Phys Lett 213:514 – 518

VandeVondele J, Krack M, Mohamed F, Parrinello M, Chassaing T, Hutter J (2005a) Quickstep: Fast and accurate density functional calculations using a mixed Gaussian and plane waves approach. Comput Phys Commun 167:103 – 128

VandeVondele J, Mohamed F, Krack M, Hutter J, Sprik M, Parrinello M (2005b) The influence of temperature and density functional models in ab initio molecular dynamics simulation of liquid water. J Chem Phys 122:014,515

VandeVondele J, Troester P, Tavan P, Mathias G (2012) Vibrational Spectra of Phosphate Ions in Aqueous Solution Probed by First-Principles Molecular Dynamics. J Phys Chem A 116:2466–2474

Wang J, Román-Pérez G, Soler JM, Artacho E, Fernández-Serra MV (2011) Density, structure, and dynamics of water: The effect of van der Waals interactions. J Chem Phys 134:024,516

Weigend F, Häser M (1997) RI-MP2: first derivatives and global consistency. Theor Chem Acc 97:331–340

Weigend F, Häser M, Patzelt H, Ahlrichs R (1998) RI-MP2: optimized auxiliary basis sets and demonstration of efficiency. Chem Phys Lett 294:143–152

Whalley E (1984) Energies of the phases of ice at zero temperature and pressure. J Chem Phys 81:4087–4092

Whitten JL (1973) Coulombic potential energy integrals and approximations. J Chem Phys 58:4496–4501

Wilhelm J, Seewald P, Del Ben M, Hutter J (2016) Large-Scale Cubic-Scaling Random Phase Approximation Correlation Energy Calculations Using a Gaussian Basis. J Chem Theory Comput 12:5851–5859